Arrays of Bolometers for Far-Infrared and Submillimeter Astronomy

D.T. Chuss, [1] C.A. Allen, [1] S. Babu, [1] D.J. Benford, [1] J.L. Dotson, [2] C.D. Dowell, [3] M. Jhabvala, [1] D.A. Harper, [4] S. Harvey Moseley, [1] R.F. Silverberg, [1] J.G. Staguhn, [1] G. Voellmer, [1] E.J. Wollack, [1]

ABSTRACT

We describe 12 x 32 arrays of semiconducting cryogenic bolometers designed for use in far-infrared and submillimeter cameras. These 12 x 32 arrays are constructed from 1 x 32 monolithic pop-up detectors developed at NASA Goddard Space Flight Center. The pop-up technology allows the construction of large arrays with high filling factors that provide efficient use of space in the focal planes of far-infrared and submillimeter astronomical instruments. This directly leads to a significant decrease in integration time. The prototype array is currently operating in the second generation Submillimeter High Angular Resolution Camera (SHARC II), a facility instrument in use at the Caltech Submillimeter Observatory (CSO). The elements of this array employ a bismuth absorber coating and quarter wave backshort to optimize the bolometer absorption for a passbands centered at 350 and 450 microns. A second array is to be installed in the High-resolution Airborne Widebandwidth Camera (HAWC), a far-infrared imaging camera for the Stratospheric Observatory for Infrared Astronomy (SOFIA). This array has been completed and is now awaiting integration into the HAWC test cryostat. HAWC is scheduled for commissioning in 2005. The HAWC array employs titanium-gold absorbers and is optimized for uniform absorption from 40 to 300 microns to accommodate all four of its far-infrared passbands. We describe the details of the HAWC array construction including the mechanical design and electrical characterization of the constituent linear arrays.

1. Introduction

In recent years, improvements in direct detection technology used in far-infrared and submillimeter astronomy have allowed astronomers to fill focal planes of telescope with larger and larger arrays of detectors that efficiently couple to astronomical radiation. Such technologies have allowed for increased observing efficiency and therefore a decrease in integration times.

The Pop-up Detector (PUD) technology developed at NASA Goddard Space Flight Center (Moseley et al. 2000) exhibits marked advantages over previous bolometer architectures. Because the electrical leads are folded out of the focal plane, it is possible to achieve filling factors close to 95%. Also, depending on the bandwidth specifications, it is possible to implement absorber strategies that achieve quantum efficiencies of close to 100% over a finite bandwidth. Finally, the architecture enables large format two-dimensional arrays to be constructed through the stacking of individual 1×32 monolithic linear arrays.

To date, two 12×32 arrays have been built using this technique. The first is currently operating in the SHARC II camera at the Caltech Submillimeter Observatory (CSO; Dowell et al., 2002). The second has recently been delivered to the University of Chicago for integration into HAWC(Harper et al. 2000), a facility imaging photometer for SOFIA (the Stratospheric Observatory for Infrared Astronomy). In section 2, we describe the two instruments. In section 3, we review pop-up technology. We discuss the constrasting absorber strategies of the two arrays in section 4. The details of the HAWC array construction are given in section 5. Finally, the current status of each detector is given in section 6.

---

[1]NASA Goddard Space Flight Center

[2]NASA Ames Research Center

[3]JPL/Caltech

[4]University of Chicago, Yerkes Observatory

2. SHARC II and HAWC

Interstellar dust at temperatures from 20 to 200 K is abundant both in our own Galaxy as well as in external Galaxies. Dust at such temperatures radiates strongly in the submillimeter and far-infrared. Specific astronomical objects that can be studied using high resolution telescopes operating at these wavelengths include galactic star formation regions, galaxy mergers, and bright ultraluminous infrared galaxies at z~1.

Because of the presence of water vapor, the atmosphere is opaque in the far-infrared and submillimeter. This fact makes ground-based astronomy at these wavelengths difficult. In the submillimeter, atmospheric "windows" at 350 and 450 μm are available during good weather at a few selective high-altitude locations, but from 40 through 300 μm, the only way to do astronomy is to place a telescope above most of the atmospheric water vapor. The Stratospheric Observatory for Infrared Astronomy (SOFIA) is NASA's next generation airborne observatory designed to provide a platform to study this wavelength regime. Offering a larger primary mirror than contemporary satellites operating at comparable wavelengths, SOFIA will achieve angular resolution in the far-infrared that will allow the most detailed maps of far-infrared sources to date.

As the facility imaging camera, HAWC will provide high resolution mapping and photometric capability to SOFIA. It will have four passbands from 40 μm through 300 μm and therefore will be able to measure spectral energy distributions (SEDs) of sources at high resolutions. This will directly lead to temperature profiles. The four HAWC passbands are given in Table 1 along with their bandwidths and angular resolutions.

The prototype array for the HAWC development effort, SHARC II (Submillimeter High Angular Resolution Camera), is currently operating at the CSO. Its primary observations are done in the 350 and 450 μm atmospheric windows; however, it is also capable of undertaking observations at 850 μm. The large aperature (10 m) of the CSO provides an angular resolution of 9″ at 350 μm. Scientifically, observations with SHARC II will serve to complement HAWC observations by providing long wavelength data at a comparable angular resolution.

The SHARC II and HAWC angular resolutions as a function of their passbands are shown and compared with other contemporary far-infrared and submillimeter instruments in Figure 1.

Two-dimensional arrays of bolometers are constructed from constituent 1×32 linear arrays (Voellmer et al. 2002). Each linear array consists of thirty-two 1 mm square bolometer membranes that are fabricated from a single piece of silicon. The bolometer membranes are ion-implanted over their full area with phosphorus and boron. Silicon straps on either side of each bolometer membrane provide mechanical support from the pixels to the frame. Aluminum traces run down both straps to provide thermal and electrical connections to the frame. Figure 2 shows a schematic of a section of a 1×32 linear array before it is folded.

The individual linear arrays are deposited with an appropriate absorber coating, and then the frames are folded back and glued to the sides of a ceramic busbar. The stress of the fold is absorbed by the torsion bars on either side of the bolometer membrane (see Fig. 2). In this way, the area to either side of the bolometer membranes is unobstructed and thus free to accommodate adjacent rows of PUDs.

Table 1. HAWC Passbands

$\lambda(\mu$m)	$\Delta\lambda/\lambda$	Angular resolution(″)
53	0.1	6
88	0.1	9
155	0.15	15
215	0.2	21
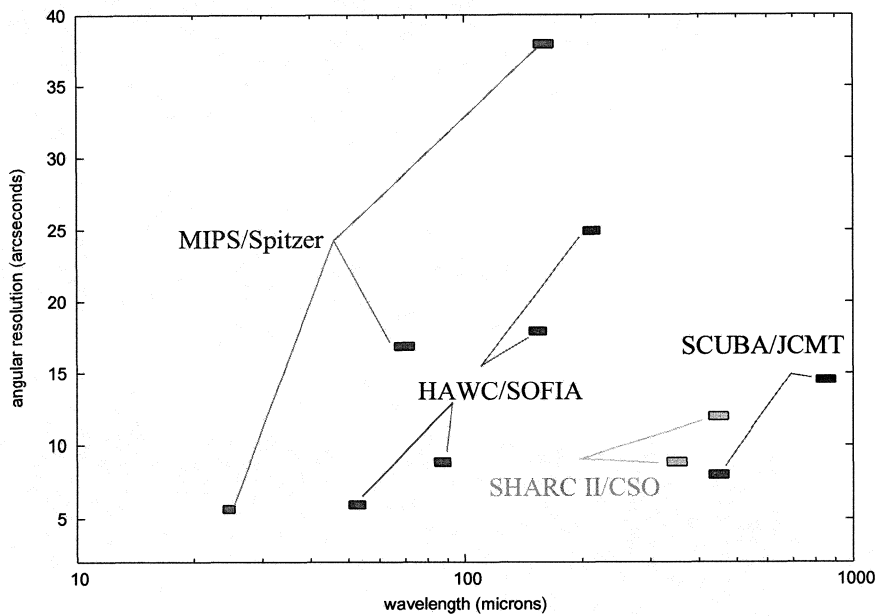
Fig. 1.— The angular resolutions and wavlength coverages of SHARC II and HAWC are compared with other contemporary far-infrared and submillimeter imagers.
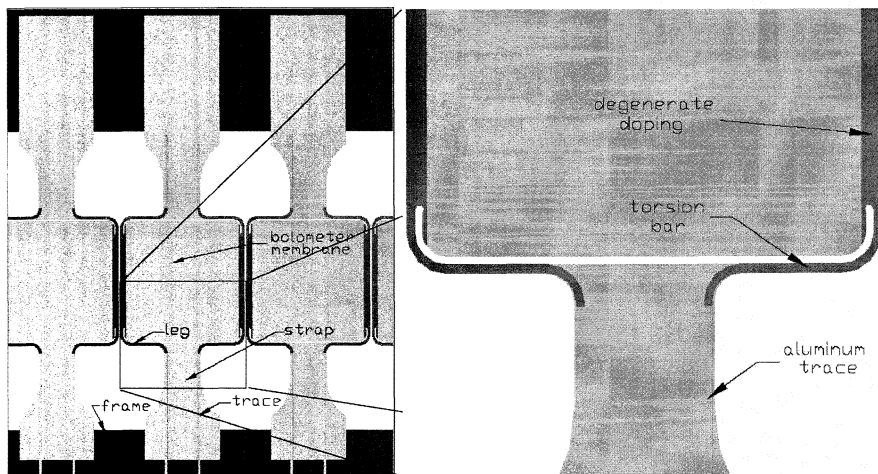
Fig. 2.— A schematic of a section of the unfolded 1×32 linear array is shown. (Dowell et al. 2002) The blowup on the right shows the details of the torsion bar that allows the straps to be folded out of the image plane.

3.   Absorber Strategies

The absorber strategies for the two arrays differ. For SHARC II, the spectral proximity of the two atmospheric windows at 350 and 450 μm allows for the efficient implementation of a resonant absorber that works well across both bands. Thus, the absorbing strategy of SHARC II consists of a 400 $\Omega/\square$ coating of bismuth absorber on the bolometer membrane accompanied by a quarter wave backshort located 100 μm behind the pixels. This configuration allows for >95% transmission across both SHARC II bands. The transmission line model and a schematic representation of this strategy are shown in the left side of Figure 3. Note the backshort is formed by the gold coated surface of the ceramic busbar. In practice, the absorption is dependent on the precision of backshort placement and surface impedance of the absorbing film on the bolometer.

In contrast, the passbands for HAWC, chosen for spectral properties of the atmosphere at 41,000 feet, span a much larger region of the spectrum. Because of the difficulties in matching these windows with a resonant backshort, the HAWC absorber strategy was chosen to maximize the bandwidth of the absorber. As shown in the right hand side of Figure 3, the bolometer membrane is coated with an optimal surface impedance of 157 $\Omega/\square$. Because bismuth has an unacceptable reactance over parts of the HAWC passband, the absorbing layer is a thin film metal alloy of titanium-gold. The gold-plated busbar is painted with an epoxy infused with carbon lamp black and 40 μm glass beads to form a cold absorber. This leads to a predicted 50% absorption that is flat across all four passbands. How close the actual absorption is to this prediction will depend on the values of the surface impedances of the Ti-Au films and the efficiency of the busbar absorber.

The titanium-gold absorbers have been found to be unstable when stored at room temperatures for periods of a year or longer. The instability manifests itself in a slow rise of the surface impedance. Thus, in order to maintain the quality of the array over the useful lifetime of HAWC, the array will be stored below -40°C when not in use. Such cold storage has been found to halt the aging process.

4.   HAWC Array Construction

The fundamental unit in the construction of the two dimensional HAWC array is the folded, absorber-coated linear array. Many such PUD linear arrays are fabricated. They then undergo a series of electrical and optical tests at cryogenic temperatures that define the criteria for downselecting the candidates to the 12 rows that make up the 384 pixel HAWC array. The rows are tested, two at a time, in a He-3 cooled test dewar. The procedures for the row testing are similar to those that were performed for SHARC II (Freund et al. 2002).

The time constants of the bolometers on each row are tested. This is done by applying a small square wave signal on top of the bias voltage. The responses of the detectors over many cycles of this signal are co-added, and a fit is done to the resulting data to determine the bolometer's time constant. For the HAWC detector, the time constants for each detector must be below 10 ms. Figure 4A shows a typical time constant data set with an exponential fit to the data.

Load curves are taken at three temperatures: 250 mK, 300 mK, and 450 mK. The current-voltage response of the detectors are found by changing the bias voltage and measuring the DC voltage across the bolometer. A sample load curve is shown in Figure 4B. The load curves provide a check to the electrical viability of each detector in a row. The electrothermal properties of the bolometers are modeled by the equations

$$R = R_o \exp \sqrt{T_o/T}, \, G = G_o(T/1K)^\beta.$$

These equations describe the resistance(R) and the thermal conductance(G) of a bolometer as functions of temperature. The determination of R_o, T_o, G_o, and β allow for optimal placement of the bolometers in the final two-dimensional configuration. In the HAWC cryostat, each adjacent pair of bolometers shares a bias voltage. Thus, by placing electrically similar rows next to one another, the six independent bias lines can be adjusted to maximize the sensitivity of the array. An electrical and thermal summary of the 12 rows of the HAWC detector is given in Table 2.
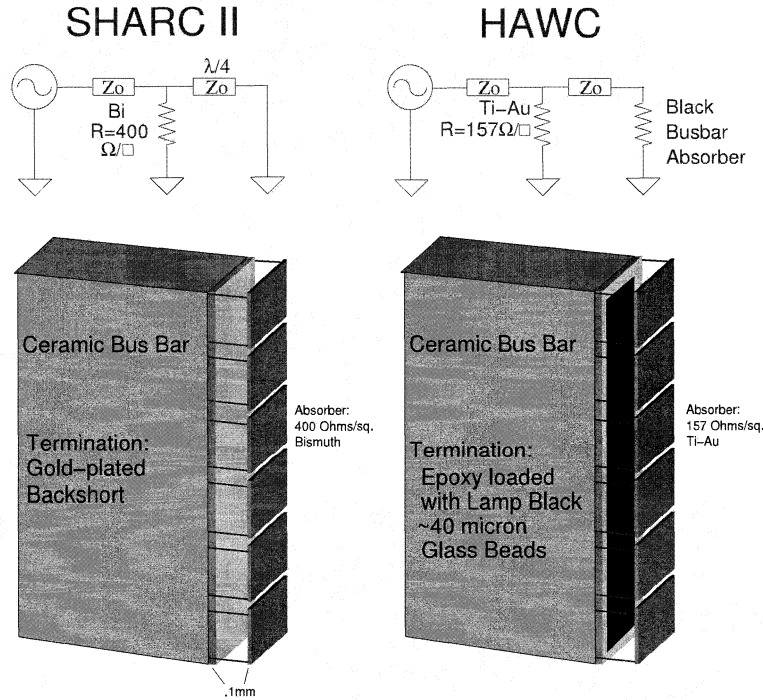
Fig. 3.— Contrasting absorber strategies for SHARC II and HAWC are shown below their respective transmission line representations. For HAWC, the absorption scheme is such as to allow for 50% absorption over the entire 40-300 μm HAWC band. The SHARC II strategy is optimized for $\sim$95% absorption over the 350 and 450 μm bands.

Table 2.   HAWC Electrical and Thermal Properties

Row	$R_o(\Omega)$ [†]	$T_o(\text{K})$ [†]	$G_o(\text{nW/K})$ [†]	β[†]	$R_{\text{surface}}(\Omega/\square)$[‡]	$\tau(\text{ms})$ [†]
1	803±342	29.5±3.1	2.95±0.61	1.93±0.16	115	6.67±0.74
2	456±31	34.3±1.7	3.73±0.15	2.06±0.06	125	6.94±1.50
3	619±175	30.0±1.2	3.93±1.95	1.98±0.31	128	9.13±2.13
4	952±158	27.7±2.4	1.48±0.41	1.93±0.03	118	8.13±1.30
5	907±152	29.0±6.4	1.88±0.62	1.66±0.31	110	5.52±1.35
6	1285±211	27.0±2.0	1.30±0.25	1.34±0.05	96	5.14±0.95
7	640±194	33.5±3.2	1.85±0.21	1.86±0.11	116	6.94±1.35
8	800±199	34.5±2.6	1.94±0.53	1.70±0.07	123	8.64±0.88
9	720±122	37.9±2.0	2.15±0.30	1.61±0.06	120	5.14±0.58
10	842±537	36.8±3.3	2.15±0.30	1.78±0.12	123	5.52±1.25
11	475±195	43.1±3.5	2.15±0.30	1.80±0.08	127	8.05±1.39
12	576±258	39.3±2.3	2.15±0.30	2.01±0.15	126	5.78±1.61

[†]Values are the mean values of the working pixels across each row. The error bars are calculated from the standard deviation of the same pixels.

[‡]The surface resistances are values obtained from witness samples immediately after the absorber deposition.

Noise tests are done on each row in order to check for rows that have excess noise. The rows are placed in the test dewar in the dark. The power spectrum of the data taken then gives the noise spectrum. Typically, baseline noise levels were found to be 20-40 nV $Hz^{-1/2}$. Given typical responsivities of 3-4×10^8 V/W, this translates to detector NEPs of 7-13×10^{-17} W $Hz^{-1/2}$. The atmospheric NEP is expected to be 2.3-6.6×10^{-16} W $Hz^{-1/2}$(Harper et al. 2000). Thus, it can be seen that these detectors will indeed provide background limited performance. A typical noise spectrum is shown in Figure 4C. The bumps that occur at various frequencies are due to external noise and microphonic sources present in the laboratory environment.

Radiation tests were also done on the HAWC arrays. These were done by pulsing an unfocused, uncalibrated thermal source (Beeman et al. 2002) behind a 350 μm filter. This source verified that submillimeter radiation couples to the bolometers. In addition, it provided an additional check on the consistency of the absorber coatings from PUD to PUD.
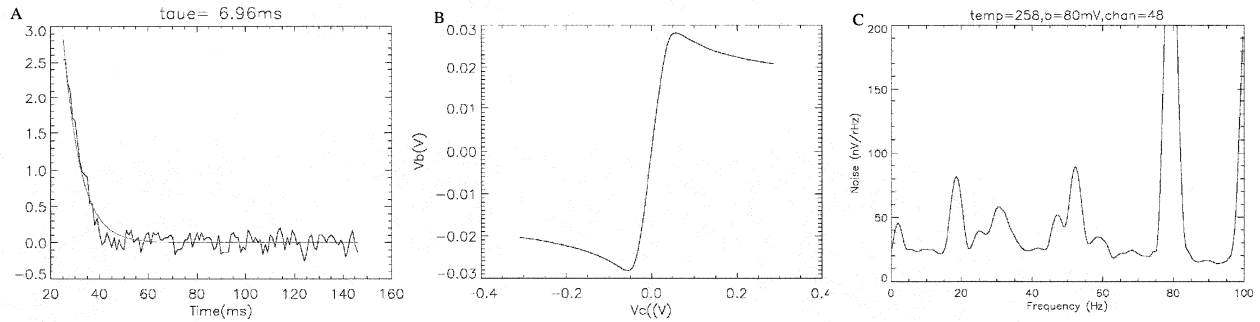
Fig. 4.— (A) Coadded time constant data are shown (jagged line) along with the best fit exponential decay (smooth line). (B) A typical load curve is given. The horizontal axis is proportional to the bias current, and the vertical axis is the voltage across the bolometer. (C) Noise results for a typical HAWC bolometer are shown.
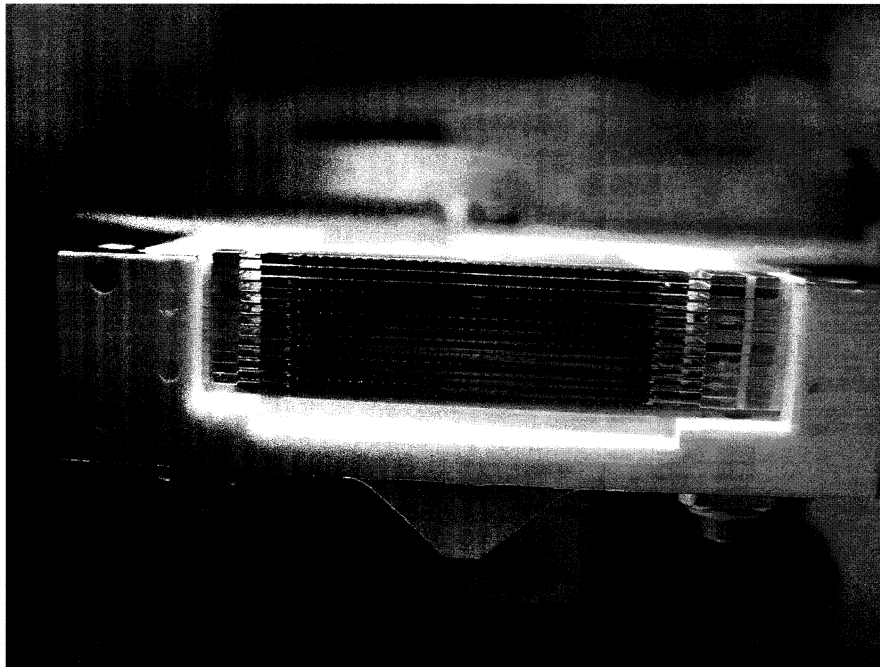
Fig. 5.— The completed HAWC array is shown.

There are two additional selection criteria that were considered. The first is that there is a 10% limit on the

number of bad pixels. Therefore, any rows containing more than 3 bad pixels were downgraded. Also, because of the concern over the absorber aging issue, rows having lower surface impedances were given higher rankings than those with higher surface impedances.

5. Current Status

The SHARC II array is currently operating at the CSO. For an example of the imaging capabilities of this instrument, see Houde et al. (2004). The HAWC array has been completed and is awaiting its integrated testing phase. A photograph of the completed HAWC array is shown in Figure 5. First light is expected for HAWC in 2005.

REFERENCES

Beeman, J., Collins, P., Hargrave, P., Pisano, G., & Haller, E. 2002, in Far-IR, Submm and mm Detector Technology Workshop, Proc. NASA Laboratory Astrophysics Workshop

Dowell, C. D., Allen, C., Babu, S., Freund, M., Gardner, M., Groseth, J., Jhabvala, M., Kovacs, A., Lis, D., Moseley, S., Phillips, T., Silverberg, R., Voellmer, G., & Yoshida, H. 2002, in Proc. SPIE, Vol. 4855, Millimeter and Submillimeter Detectors for Astronomy, ed. T. Phillips & J. Zmuidzinas, 73

Freund, M., Silverberg, R., Ponce, V., Allen, C., Sappington, C., Moseley, S., Harper, D., Loewenstein, R., & Dowell, C. 2002, in Proc. SPIE, Vol. 4855, Millimeter and Submillimeter Detectors for Astronomy, ed. T. Phillips & J. Zmuidzinas

Harper, D., Allen, C., Amato, M., Ames, T., Bartels, A., Casey, S., Derro, R., Evans, R., Gatley, I., Heimsath, S., Hermida, A., Jhabvala, M., Kastner, J. H., Loewenstein, R., Moseley, S., Pernic, R., Rennick, T., Rhody, H., Sanford, D., Shafer, R., Shirron, R., Voellmer, G., Wang, S., & Wirth, J. 2000, in Proc. SPIE, Vol. 4014, Airborne Telescope Systems, ed. R. Melugin & H. Roesner, 43–53

Houde, M., Dowell, C., Hildebrand, R., Dotson, J., Vaillancourt, J., Phillips, T., Peng, R., & Bastien, P. 2004, ApJ, 604, 717

Moseley, S., Dowell, C., Allen, C., & Phillips, T. 2000, in ASP Conference Series, Vol. 217, Imaging at Radio through Submillimeter Wavelengths, ed. J. Mangum & S. Radford, 140–149

Voellmer, G., Allen, C., Amato, M., Bartels, A., Benford, D., Derro, R., Dowell, C., Harper, D., Moseley, S., Shirron, P., Smith, W., & Staguhn, J. 2002, in Proc. SPIE, Vol. 4855, Millimeter and Submillimeter Detectors for Astronomy, ed. T. Phillips & J. Zmuidzinas